The computational kernel of the DS-WRELAX algorithm involves obtaining the estimates $\{\hat{\tau}_\ell, \hat{\sigma}_\ell\}$ of $\{\tau_\ell, \sigma_\ell\}$ using eqn. 8, which require that the global maximum of the following function be searched for:

$$J(\tau_\ell, \sigma_\ell) \triangleq \mathbf{y}_\ell^H \cdot \mathbf{s} \cdot (\mathbf{s}^H \cdot \mathbf{s})^{-1} \cdot \mathbf{s}^H \cdot \mathbf{y}_\ell \qquad (10)$$

$J(\tau_\ell, \sigma_\ell)$ is referred to as the CLF in [1]. In general, maximising $J(\tau_\ell, \sigma_\ell)$ involves a 2D search. However, for some kinds of signals, the CLF defined in eqn. 10 contains special shapes that can be exploited to significantly reduce the computational overhead. For example, for the HFM signals widely used in active sonar, the CLF has a very narrow ridge [1, 2]. In this case, the original 2D search problem can be reduced into two 1D searches (see [1, 2] for details). In this way, the efficient FML algorithm for a single target was extended to the multiple target case more efficiently than was the case in [2].

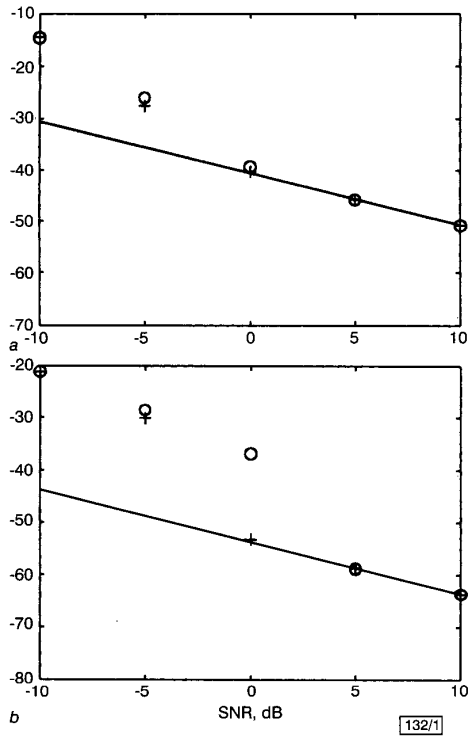

Fig. 1 *Comparison of MSEs obtained via DS-WRELAX and FML algorithms with corresponding CRBs for τ_1 and σ_1*

a τ_1
b σ_1
\+ DS-WRELAX
○ FML
——— CRB

Numerical results and discussions: In this Section, we provide a numerical example to enable a comparison to be made of the performance of the proposed DS-WRELAX algorithm with the similarly structured FML algorithm [2] and the corresponding Cramer-Rao bounds.

Consider the same transmitted signal as used in [1, 2], where $s(t)$ is a wideband HFM signal defined as

$$s(t) = \begin{cases} e^{ja\ln(1-kt)}g(t) & 0 \le t \le T \\ 0 & \text{otherwise} \end{cases} \qquad (11)$$

where T is the transmitted signal duration, $k = (f_2 - f_1)/(f_2T)$, $a = (-2\pi f_1)/k$ with f_1 and f_2 denoting the initial and final frequencies, respectively, and $g(t)$ denotes a window function as defined in [1, 2]. In our numerical examples presented below, we have set T = 2s, f_1 = 186Hz, f_2 = 314Hz, T_{obs} = 4s, and the sampling rate is 1/512s.

Suppose that the received signal is composed of two echoes with the following parameters: $\alpha_1 = 0.2e^{j\pi/2}$, τ_1 = 0.5s, σ_1 = 1.05, $\alpha_2 = 0.1902e^{j\pi/4}$, τ_2 = 0.54s, and σ_2 = 0.95. The signal-to-noise ratio (SNR) of the ℓth echo is defined as $SNR_\ell = \|\alpha_\ell \cdot \mathbf{s}(\tau_\ell, \sigma_\ell)\|^2/(N \cdot \sigma_e^2)$, where σ_e^2 denotes the noise variance. Under the above assumption, $SNR_1 = SNR_2$. The mean squared errors (MSEs) of the delay and Doppler scale estimates of the first echo obtained via DS-WRELAX and those obtained via FML are compared with the corresponding Cramer-Rao bounds (CRBs) in Fig. 1 against SNR. (The results for the second echo are similar and hence are not shown here.) The MSEs were obtained through 300 Monte Carlo trials. From Fig. 1 it can be seen that the MSEs of the estimates obtained via both algorithms can reach the corresponding CRBs at high SNR, and the DS-WRELAX algorithm has a much lower SNR threshold than that of the FML algorithm. Further investigation results show that the above performance difference derives from their difference in global convergence properties.

Acknowledgments: This work was supported in part by the 863 High-Tech Project of China under contract 863-308-19-01-(3), and by the National Natural Science Foundation of China under grant 69902009.

7 February 2000
Electronics Letters Online No: 20000634
DOI: 10.1049/el:20000634

Zhigang Su and Renbiao Wu (*Communications and Signal Processing Research Laboratory, Civil Aviation University of China, Tianjin 300300, People's Republic of China*)

E-mail: wrbwm@public.tjuc.com.cn

Renbiao Wu: Corresponding author

References

1 TUFTS, D.W., GE, H., and UMESH, S.: 'Fast maximum likelihood estimation of signal parameters using the shape of the compressed likelihood function', *IEEE J. Oceanic Eng.*, 1993, **18**, (4), pp. 388–400

2 UMESH, S.: 'Fast maximum likelihood estimation of parameters in crowded signal environments'. PhD Dissertation, University of Rhode Island, Kingston, RI, August 1993

3 LI, J., and WU, R.: 'An efficient algorithm for time delay estimation', *IEEE Trans.*, 1998, **SP-46**, (8), pp. 2231–2235

High-speed focusing algorithm for circular synthetic aperture radar (C-SAR)

M. Bara, L. Sagués, F. Paniagua, A. Broquetas and X. Fàbregas

A new algorithm is presented which is capable of generating very fast high-resolution images for circular synthetic aperture radar (C-SAR) systems. Its main characteristic is that it allows the processing of data from such ground-based radars in near real-time, as validated with some experimental results.

Introduction: A circular synthetic aperture radar (C-SAR) system based on a short-range scatterometer was presented in [1], where the technical configuration of the equipment as well as the processing software was described. In principle, its major applications are buried object detection or the study of surface scattering, and also height profile extraction by means of interferometric techniques [2]. Moreover, it can be an excellent tool for those applications in which it is feasible to extrapolate the generated data to spaceborne or airborne SAR platforms. C-SAR systems use a continuous-wave stepped frequency scan, transmitted by an antenna which describes a circular trajectory around a rotating vertical mast (Fig. 1). Considering synthetic aperture principles, the received data can be processed in order to enhance the cross-range resolution. One possibility is to employ an algorithm based on inverse SAR techniques [1], which applies a matched filter to focus every pixel of the input matrix in order to obtain the final image. However, this procedure is relatively slow if the considered application requires that the data be made available at high speed, as occurs during outdoor measurements. In this Letter we present

a new procedure (called Quick-CSAR) for this case, which is based on the chirp scaling (CS) algorithm [3] originally developed for conventional linear SAR sensors. The traditional approach has been modified to make feasible the use of circular geometries and continuous-wave radars. Several experimental results are presented to prove the achieved precision as well as the applicability of the new algorithm in real-time outdoor scenarios.

Quick-CSAR processor: The received signal from a single scatterer is given by

$$S(f,\phi_a) = A_0 \cdot \prod\left(\frac{f}{B_\tau}\right) \cdot a(\phi_a - \phi_s) \times \exp\left[-j\frac{4\pi}{c}(f+f_0)\cdot R_{AS}(\phi_a;\rho_s,\phi_s)\right] \quad (1)$$

since the measurements are performed at azimuth angle ϕ_a and range frequency f around the centre frequency f_0. The bandwidth is represented by B_τ, while (ρ_s, ϕ_s) is the target position, $a(\cdot)$ is the azimuth antenna pattern and A_0 is an arbitrary complex constant. The function $R_{AS}(\cdot)$ is the distance between the antenna and the scatterer along the azimuth angle dimension:

$$R_{AS}(\phi_a;\rho_s,\phi_s) = \sqrt{R^2+\rho_s^2+h^2-2R\rho_s\cos(\phi_s-\phi_a)} \simeq \sqrt{(\rho_s-R)^2+h^2+R\rho_s(\phi_a-\phi_s)^2} \quad (2)$$

where R and h are the antenna arm and height, respectively. The approximation of eqn. 2 is valid for relatively small antenna beamwidths as in the C-SAR case. The main problem to be solved by the focusing algorithm is to correct the range migration effect, which is characterised by the following range distance function in the azimuth frequency (f_ϕ) domain:

$$R(f_\phi) = \frac{\sqrt{(\rho_s-R)^2+h^2}}{\sqrt{1-\left(\frac{\lambda\cdot f_\phi}{2\cdot\sqrt{R\cdot\rho_s}}\right)^2}} \quad (3)$$

The key point of the proposed algorithm is the introduction of the FM modulation, which is an operation that needs to be carried out at this stage. The data are multiplied by a quadratic phase function with the form

$$\Phi_0(f) = \exp\left(j\cdot\pi\cdot\frac{f^2}{K}\right) \quad \text{where } K = \frac{B_\tau}{\tau_0} \quad (4)$$

The constant K is the FM rate and τ_0 is the duration of the introduced chirp pulse. As a result of this operation, the signal can be treated with the CS algorithm, assuming the differences between the circular and linear expressions. Basically, the utilisation of the chirp enables the effect of range migration to be corrected for over the swath by exploiting the chirp properties [3]. A final step of radiometric correction has also been included in order to avoid the effects of the target position and the radiation antenna patterns.

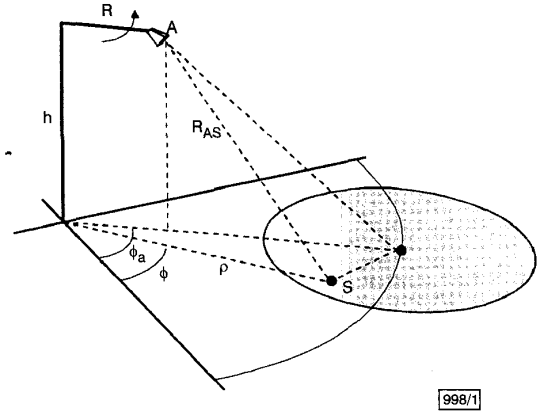

Fig. 1 *Circular SAR geometry*

Measurement results: Several results are presented in this Section to enable a comparison to be made of the performance of the new approach with that of the previous approach. The presented measurement was performed with HH polarisation and covered the frequency range 8 – 12GHz, with a frequency interval of 10MHz. The antenna arm was 1m, while the height was 1.87m with an off-nadir elevation angle of 50°. The computational times were measured with a portable personal computer (AMD K6-II 333MHz with 64Mbyte RAM) which forms part of the outdoor equipment. Fig. 2 shows the reconstructed image (polar co-ordinates) obtained by a Quick-CSAR processor, corresponding to two identical small trihedrals and a metallic sphere placed above an absorbent surface. This measure shows that the objects have the same position and relative reflectivity with both algorithms, whereas the spatial resolution only degrades by < 3%. The new method also presents quasi-space invariancy as well as uniform sensitivity. The main difference between both algorithms is the computational time. The original C-SAR approach took 18 min, while the new approach delivered the image in 32s. This difference in computational time is greater in measurements where the raw data matrix is larger, or a greater number of points in the ground range are required.

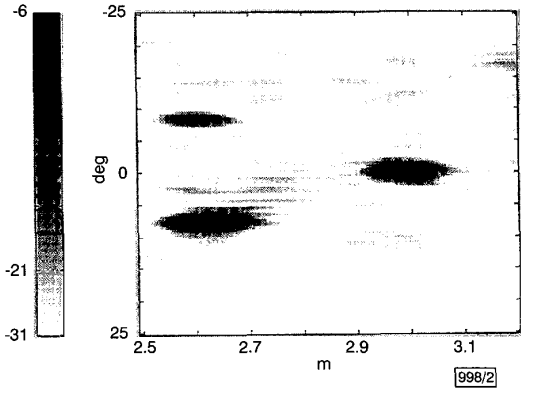

Fig. 2 *Quick-CSAR reflectivity image (two trihedrals and one sphere)*

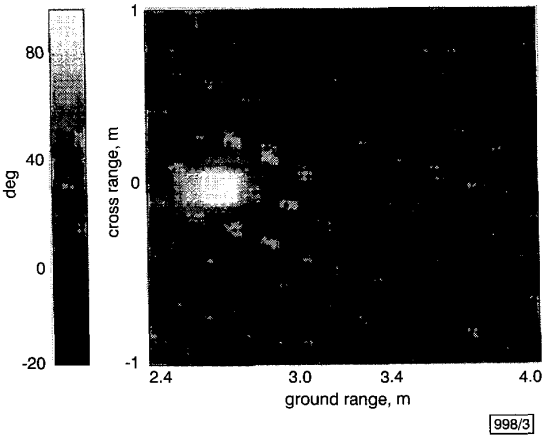

Fig. 3 *Quick-CSAR interferogram (without flat-Earth term)*

Several data sets with different baseline distances were recorded in order to also verify the utility of the processor for interferometric applications. The measured terrain was a dielectric rough surface of gravel made up of a small mountain 25cm high. Fig. 3 depicts the averaged phase information (interferogram) for a 4 cm baseline and a frequency range between 8 and 12GHz obtained with the new algorithm. The gravel pile appears clearly on the left, where a mean height error of 4.4cm has been calculated after the phase to height conversion. This result proves the phase preservation of the presented algorithm.

Conclusions: A new circular synthetic aperture radar processor has been described and evaluated. Its main characteristic is its low computational time without loss of resolution, precision and phase accuracy. It enables the recorded data during outdoor campaigns to be checked.

Acknowledgments: This work has been supported by the Comissionat per Universitats i Recerca (CIRIT) and the Spanish Commission for Science and Technology (CICYT) TIC99-1050-C03-01.

22 March 2000
Electronics Letters Online No: 20000633
DOI: 10.1049/el:20000633

M. Bara, L. Sagués, F. Paniagua and X. Fàbregas (*Department of Signal Theory and Communications, Universitat Politècnica de Catalunya (UPC), Campus Nord, C/ Jordi Gironi, 1-3, 08034 Barcelona, Spain*)

E-mail: mabara@tsc.upc.es

A. Broquetas (*Institute of Geomatics, Parc de Montjuïc, s/n, 08038 Barcelona, Spain*)

References

1 BROQUETAS, A., DE PORRATA, R., SAGUÉS, L., FÀBREGAS, X., and JOFRE, L.: 'Circular synthetic aperture radar (C-SAR) system for ground-based applications', *Electron. Lett.*, 1997, **33**, (11), pp. 988–989

2 SAGUÉS, L., BARA, M., BROQUETAS, A., and FÀBREGAS, X.: 'An interferometric circular synthetic aperture radar (InCSAR) system for ground-based applications'. NATO RTO Meeting Proc. High Resolution Radar Techniques, 1999, pp. 64.1–64.10.

3 RANEY, R.K., RUNGE, H., BAMLER, R., CUMMING, I.G., and WONG, F.H.: 'Precision SAR processing using chirp scaling', *IEEE Trans. Geosci. Remote Sens.*, 1994, **32**, (4), pp. 786–799

Measurement of diffraction radar cross-section (RCS)

F.C. Smith

A technique is described for measuring the RCS of 2D (two-dimensional) diffracting sources. The measured and predicted diffraction RCS of a conducting halfplane edge and a gap in an otherwise infinite conducting plane are presented. The technique may be used to measure the diffraction coefficient of an impedance discontinuity.

Introduction: The problem of predicting the radar cross-section (RCS) of 2D diffracting sources is amply addressed in the published literature. After specular reflection, diffraction is often the largest contributor to the RCS of a target [1]. Notwithstanding the theoretical interest in diffraction, very few techniques are available to the experimenter for measuring microwave diffraction in isolation from other scattering phenomena. Microwave diffraction has, of course, been measured in conjunction with other scattering mechanisms, for example [2]. Some diffraction-only data from buildings have been published [3, 4], though the measurement techniques used are not appropriate to characterising 2D RCSs. Diffraction-based RCS data of a quasi-2D material/material discontinuity are given in [5]. Here, the sample is mounted on a low-observable (LO) diamond-shaped test piece. The shape of the test piece reduces measurement error; however, discrepancies between predicted data and measured data of between 2 and 5dBm^2 are still observed. The diamond-shaped test piece is replaced with a triangular test piece if the diffracting source is a halfplane edge. Remarks by the authors of [3, 5] highlight the paucity of measured data relating to diffraction sources.

Experimental method for measuring 2D RCS: The 2D RCS (σ_{2D}) can be expressed as

$$\sigma_{2D} = 2\pi r \lim_{r \Rightarrow \infty} \frac{E_s^2}{E_i^2} \qquad (1)$$

where E_s and E_i are, respectively, the scattered field at the observation point and the incident field at the scatterer; r is the distance between the scatterer and the observation point.

Fig. 1 shows the schematic diagram of an off-axis quasi-optic reflectometer designed to measure σ_{2D}. The reflectometer utilises a corrugated conical horn and elliptical mirror to produce a near mono-modal Gaussian beam at the focal plane of the mirror. The measured diameter of the beam's –50dB contour (relative to the maximum) is 258mm at the focal plane of the mirror (at 10 GHz); the mirror's aperture is ~440mm. Samples appear to be 2D to the interrogating wavefront provided that they are greater than ~300mm in length and are structurally and electromagnetically invariant along one axis.

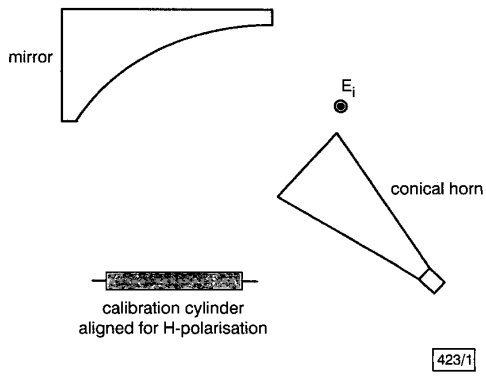

Fig. 1 *Compact range for measuring 2D radar cross-section*

The off-axis reflectometer is subject to the normal one-port errors. Tracking errors and the unknown quantity r/E_i^2 in eqn. 1 are eliminated through the measurement of a conducting circular cylinder the 2D RCS of which is calculable analytically. Directivity errors are eliminated by subtracting data recorded with no sample present. Mismatch errors are removed through the use of time-domain filtering. All mismatch errors for the 2D RCS range are temporally discrete and may be removed without the subjective use of time domain filters.

Measured results using 2D compact range: All data shown here are monostatic data calibrated using measurements from a circular conducting cylinder of radius 2.5mm. Predicted data for all flat-plate measurements were obtained using a 2D finite difference time domain (FDTD) code. The procedure for isolating edge diffracted fields in the FDTD model from other scattering phenomena is described in [6]. The FDTD data reported here have an estimated worst case uncertainty of ± 0.15dBm [6].

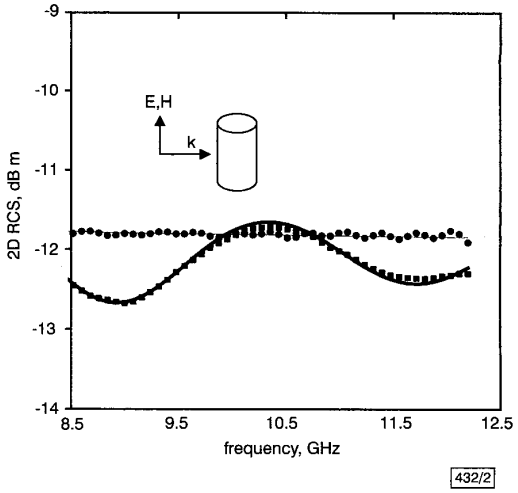

Fig. 2 *Measured and predicted 2D RCS of circular conducting cylinder of diameter 40.8mm*

■ H measured
— H predicted
● E measured
—— E predicted

The measurement technique has been validated for E and H polarisation by measuring several circular aluminium cylinders. Fig. 2 shows the measured and predicted 2D RCS for the E and H polarisation of an aluminium circular cylinder of diameter 40.8mm.